New insights into the involvement of residue D1-V185 in Photosystem II function in *Synechocystis 6803* and *Thermosynechococcus vestitus*.

Alain Boussac[a], Julien Sellés[b], Miwa Sugiura[c], Robert L. Burnap[d]

[a] Institut de Biologie Intégrative de la Cellule, UMR9198, CEA Saclay, 91191 Gif-Sur-Yvette, France. alain.boussac@laposte.net

[b] Institut de Biologie Physico-Chimique, UMR CNRS 7141 and Sorbonne Université, 13 rue Pierre et Marie Curie, 75005 Paris, France. julien.selles@ibpc.fr

[c] Proteo-Science Research Center, Department of Chemistry, Graduate School of Science and Technology, Ehime University, Bunkyo-cho, Matsuyama, Ehime 790-8577, Japan. miwa.sugiura@ehime-u.ac.jp

[d] Department of Microbiology and Molecular Genetics, Oklahoma State University, Stillwater, OK 74078. rob.burnap@okstate.edu

ORCID numbers :

Alain Boussac: 0000-0002-3441-3861

Miwa Sugiura: 0000-0002-4232-5941

Julien Sellés: 0000-0001-9262-8257

Robert L. Burnap: 0000-0001-6715-5961

Key words :

Photosystem II, D1-V185, EPR, proton release, S-state cycle, spin state, Mn_4CaO_5 cluster

Abbreviations:

Photosystem II, PSII; Chl, chlorophyll; Chl_{D1}/Chl_{D2}, monomeric Chl on the D1 or D2 side, respectively; MES, 2-(*N*-morpholino) ethanesulfonic acid; P_{680}, primary electron donor; P_{D1} and P_{D2}, individual Chl on the D1 or D2 side, respectively, which constitute a pair of Chl with partially overlapping aromatic rings; Phe_{D1} and Phe_{D2}, pheophytin on the D1 or D2 side, respectively; PPBQ, phenyl *p*–benzoquinone; Q_A, primary quinone acceptor; Q_B, secondary quinone acceptor; Tyr_Z, the tyrosine 161 of D1 acting as the electron donor to P_{680}; WT*3, *T. elongatus* mutant strain deleted $psbA_1$ and $psbA_2$ genes and with a His-tag on the carboxy terminus of CP43. EPR, Electron Paramagnetic Resonance.

Abstract

The effects of D1-V185T and D1-V185N mutations in Photosystem II (PSII) from *Thermosynechococcus vestitus* (formerly *T. elongatus*) and *Synechocystis* 6803, respectively, were studied using both EPR and optical kinetics. EPR spectroscopy reveals the presence of a S_2 state in a high spin configuration (S_2^{HS}) and in a low spin configuration (S_2^{LS}) in both mutants. In contrast to the S_2^{HS} in the wild type at high pH, the S_2^{HS} state in the D1-V185T mutant does not progress to the S_3 state at 198 K. This inability is likely due to alterations in the protonation state and hydrogen-bonding network around the Mn_4CaO_5 cluster. Optical studies show that these mutations significantly affect proton release during the S_3-to-S_0 transition. While the initial fast proton release associated with $Tyr_Z^{\bullet}$ formation remains unaffected within the resolution of our measurements, the second, and slower, proton release is delayed, suggesting that the mutations disrupt the hydrogen-bonding interactions necessary for efficient deprotonation of substrate water (O6). This disruption in proton transfer also correlates with slower water exchange in the S_3 state, likely due to non-native hydrogen bonds introduced by the threonine or asparagine side chains at position 185. These findings point to a critical role of D1-V185 in regulating both proton transfer dynamics and water binding, underscoring a complex interplay between structural and functional changes in PSII.

Introduction

Oxygenic photosynthesis in cyanobacteria, algae and higher plants converts solar energy into the chemical bonds of sugars and of dioxygen [1]. Photosystem II (PSII) begins this process by splitting water to obtain electrons in the form of reduced quinone, while generating a proton gradient and releasing O_2. The mature PSII binds 35 chlorophylls *a* (Chl-*a*), 2 pheophytins (Phe-*a*), 1 membrane b-type cytochrome, 1 extrinsic c-type cytochrome (in cyanobacteria and red algae), 1 non-heme iron, 2 plastoquinones (Q_A and Q_B), the Mn_4CaO_5 cluster, 2 Cl^-, 12 carotenoids and 25 lipids [2,3]. In the cyanobacterium *Synechocystis sp.* PCC 6803 a 4th extrinsic subunit, PsbQ, has also been found in addition to PsbV, PsbO and PsbU [4].

Among the 35 Chl-*a*, 31 are antenna Chls. When one is excited, the excitation energy is transferred to other chlorophylls until it reaches the key pigments in the photochemical reaction centre: 4 Chl-*a* molecules, P_{D1}, P_{D2}, Chl_{D1}, Chl_{D2} and 2 Phe-*a* molecules, Phe_{D1} and Phe_{D2}. A few picoseconds after the formation of the excited Chl_{D1}*, a charge separation occurs resulting ultimately in the formation of the $Chl_{D1}^+Phe_{D1}^-$ and then $P_{D1}^+Phe_{D1}^-$ radical pair states, *e.g.* [5,6]. Formation of the $Chl_{D1}^+Phe_{D1}^-$ radical pair was recently defined as a fast pathway (short-range charge-separation) in contrast with a slow pathway with $P_{D1}P_{D2}$ as the initial donor (long-range charge separation) that would result directly in the formation of the $P_{D1}^+Phe_{D1}^-$ radical pair [7].

After the charge separation, P_{D1}^+ oxidizes Tyr_Z, the Tyr161 of the D1 polypeptide, which then is reduced by the Mn_4CaO_5 cluster. The electron on Phe_{D1}^- is then transferred to Q_A, the primary quinone electron acceptor, and then to Q_B, the second quinone electron acceptor. Whereas Q_A can be only singly reduced under normal conditions, Q_B accepts two electrons and two protons before to leave its binding site and to be replaced by an oxidized Q_B molecule from the membrane plastoquinone pool, see for example [1,8–12] for a non-exhaustive list of recent reviews on PSII function. The Mn_4CaO_5 cluster, oxidized by the $Tyr_Z^\bullet$ radical formed after each charge separation, cycles through five redox states denoted Sn, where n stands for the number of stored oxidizing equivalents. The S_1-state is stable in the dark, which makes S_1 the preponderant state after dark-adaptation and the decay of the S_3 and S_2 states. When the S_4-state is formed, after the 3rd flash of light given on dark-adapted PSII, two water molecules bound to the cluster are oxidized, O_2 is released and the S_0-state is reformed, [13,14].

Thanks to the advent of serial femtosecond X-ray free electron laser crystallography and cryo-EM spectroscopy, structures of the Mn_4CaO_5 cluster have been resolved in the dark-adapted S_1 state and in the S_2 and S_3 states in a redox state as close as possible to those expected taking into account the misses under flash illumination. In the S_1 state, *i.e.* in the $Mn^{III}{}_2Mn^{IV}{}_2$ redox state, the Mn_4CaO_5 structure resemble a distorted chair including a μ-oxo-bridged cuboidal Mn_3O_4Ca unit with a fourth Mn attached to this core structure via two μ-oxo bridges involving the two oxygen's O4 and O5 [2]. Recently, important progresses have been done in the resolution of the crystal structures in the S_2, S_3 [15-17] and S_0 states [15,16]. The structural changes identified in the S_1 to S_2 transition and those more pronounced in the S_2 to S_3 transition are too numerous to detail them in a few lines. Very briefly, these works show that, in S_2, the changes in the structure of the cluster are minor and more or less correspond to those expected for the valence change of the Mn4 from +III to +IV in the context of the high-valence option. Importantly, water molecules in the “O1” and “O4” channels, defined as such because they start from the O1 and O4 oxygens of the cluster, appeared localized slightly differently in S_2 and S_1. In contrast, in the S_2 to S_3 transition, major structural changes have been detected together with the insertion of a 6th oxygen (named either O6 or Ox), possibly that one of W3 originally bound to the Ca site, bridging Mn1 and Ca. This oxygen is supposed to correspond to the second water substrate molecule and is close to the bridging oxygen O5 supposed to be the first water substrate molecule [18]. An important movement of the Glu189 residue would allow its carboxylate chain to make a hydrogen bond with the protonated form of the 6th oxygen in S_3 [16,17].

EPR studies show the existence of more than one structural forms of S_1, S_2, and S_3.The two S_1 EPR signals seen with a parallel mode detection at $g \sim 4.8$ and $g \sim 12$ [19–21] were attributed to an orientational Jahn–Teller isomerism of the dangler Mn4 with the valence +III [22].

In S_2, at least two EPR signals can be detected at helium temperatures. The first one has a low-spin $S = 1/2$ value, S_2^{LS}, characterized by a multiline signal made up of at least 20 lines separated by approximately 80 gauss, centered at $g \sim 2.0$ and spread over roughly 1800 gauss [23–25]. The second configuration of S_2 is a high-spin ground state, S_2^{HS}, with $S \geq 5/2$. In plant PSII, S_2^{HS} may exhibit either a derivative-like EPR signal centered at $g \sim 4.1$ [26,27] or more complex signals at higher g values [28,29]. In cyanobacterial PSII, the $g \sim 4.1$ signal is not detected. Instead, the S_2^{HS} EPR signal has a derivative-like shape centered at $g \sim 4.8$ [30,31].

In a computational work [32], it was proposed that the $g \sim 4.1$ signal have almost the same coordination and environment as the $g \sim 2.0$ signal but with the Mn^{III} ion located on the dangler Mn4 in the S_2^{HS} state instead on the Mn1 in the S_2^{LS} state. This valence swap would be accompanied by a moving of the oxygen O5 from a position where it links the Mn4, Mn3 and the Ca in the S_2^{LS} configuration to a position where it bridges the Mn1, Mn3 and Ca ions in the S_2^{HS} configuration resulting into the so called closed cubane structure. However, this structure proposed for the S_2^{HS} configuration has never been observed that is not surprising since most of the 3D studies have been done in cyanobacteria in which the $g \sim 4.1$ signal is not observed.

In other computational works [33-35] the authors arrived at a very different model in which, starting from the S_2^{LS} configuration, the protonation of O4 would lead to an $S = 5/2$ ground state when W1, one of the two water molecules with W2 bound to the dangler Mn4, is present as an aquo ligand. The further deprotonation of W1 to form a hydroxo ligand would then give rise to an $S = 7/2$ ground state [33-35]. In the same works, it was proposed that the form $S = 7/2$ was probably that needed to progress to S_3. Importantly, the S_2^{HS} form detected at $g \sim 4.8$ form, *i.e.* the $S = 7/2$ form that corresponds to an open cubane structure in [33-35], is able to progress to S_3 at low temperatures [30,31] (whereas in plant PSII the g ~ 4.1 signal is unable to do it [36]).

From an EPR point of view, the S_3-state also exhibits some heterogeneities. The majority of centers exhibits a spin $S = 3$ ground state [37-39]. In this $S = 3$ configuration, the four Mn ions of the cluster have a Mn^{IV} formal oxidation state with an octahedral ligation sphere in an open cubane structure [39]. In this model, the dangler Mn^{IV} ($S = 3/2$) is antiferromagnetically coupled to the open cubane motif Mn^{IV}_3 with a total spin value $S = 9/2$. The remaining centers are EPR invisible, *e.g.* [40]. A third S_3 configuration with a broadened S_3 signal was identified with ELDOR-detected NMR (EDNMR) in the presence of glycerol [41,42] and in PSII/Sr [43]. Although in [43] the authors did not completely rule out the presence of a closed cubane, five-coordinate S_3 form, at the origin of this EPR signal, they favored a perturbation of the coordination environment at Mn4 and/or Mn3 in an open cubane S_3 structure induced by glycerol. With X-and Q-band EPR experiments performed in the S_3-state of plant PSII, both in the perpendicular and parallel modes, a high-spin, $S = 6$, was proposed to coexist with the $S = 3$ configuration. This $S = 6$ form was attributed to a form of S_3 without O6/Ox bound and with the Mn^{IV}_3 part of the cluster in ferromagnetic interaction with the unsaturated dangler Mn^{IV} [42]. These two forms of S_3 are, however, not detected by X-band EPR, and it seems unlikely that they correspond to the EPR invisible S_3 mentioned

above. Indeed, these new S_3 signals described in [41,42] are detectable in the presence of glycerol and methanol, whereas the formation of the $(S_2Tyr_Z\bullet)'$ state upon a near-IR illumination in the centers in S_3 defined as EPR invisible is inhibited in the presence of glycerol (and in the presence of methanol in plant PSII) [44,45].

In cyanobacterial PSII/Sr [43], a proportion of centers exhibited a pulsed W-band field-swept S_3 spectrum much broader than in PSII/Ca. This signal was proposed to be present in centers containing a 5-coordinate Mn ion in centers in which no water binding event takes place during the S_2 to S_3 transition. It was therefore proposed that, in these centers, the oxidation event would precede the water binding. Computational works also suggested heterogeneities in S_3 [46–48] with also a $S = 6$ spin value [48].

None of the heterogeneities described above were detected in the crystallographic structures of S_2 and S_3 known to date (see references above). In addition, recent high-energy resolution fluorescence detected X-ray Absorption Spectroscopy together with QM calculations ruled out the presence of either peroxo or oxo/oxyl level intermediate to explain the S_3 heterogeneity [49].

It is quite possible that some of the structural differences that cause the differences identified in EPR are too small to be detectable given the resolution of the crystallographic data. This at least shows, if it were necessary, that spectroscopy remains an indispensable complement to crystallography.

The EPR data summarized above describes a static view of the trapped configurations. Kinetically, it is well documented that the transition from S_2 to S_3 involved at least two phases. The fastest phase, with a $t_{1/2} \leq 25$ µs, is attributed to a proton transfer/release. This fast phase precedes the electron transfer from S_2 to the $Tyr_Z^{\bullet}$ with a $t_{1/2} \leq 300$ µs [50–54], and the binding of O6/Ox to the Mn1, *e.g.* [55]. It was proposed that the fast phase could correspond to the release of a proton in an intermediate step $S_2^{LS}Tyr_Z^{\bullet} \rightarrow S_2^{HS}Tyr_Z^{\bullet}$ before the $S_2^{HS}Tyr_Z^{\bullet} \rightarrow S_3^{S=3}$ transition occurs [30]. The existence of intermediate states in the S_2 to S_3 transition was tracked by following, at room temperature, the structural changes in the S_2 to S_3 transition in the µs to ms time-range after the 2nd flash [17,55]. In these works, no indication was found for a closed cubane intermediate. However, there was no conclusion on the spin state of the intermediate forms of S_2 able to progress to S_3. By definition, an intermediate state has a low concentration that makes its detection difficult and the question of the existence of a high spin intermediate state in the S_2 to S_3 transition remains. In particular, it is questionable whether the fast phase observed in this transition corresponds to a proton release/movement associated with the formation of a S_2^{HS} state, as has been suggested [30,54]. In such a model, we would

expect to detect a change in the flash pattern of the proton release in conditions in which the S_2^{HS} EPR signal is the flash-induced state. This was indeed the case since we have kinetically detected a proton release in PSII/Ca and PSII/Sr at pH 6.0 and 7.0, knowing that at pH 7.0, in PSII/Sr in contrast to PSII/Ca, half of the centers exhibit the S_2^{HS} signal at g ~ 4.8 able to progress to S_3 at low temperatures [36].

Independently of the pH effect and Ca/Sr exchange, several mutations, the list being too long for making it here, in the first and second coordination sphere of the Mn_3O_4Ca unit strongly perturb the water splitting process. One of these mutants is the D1-V185N mutant in *Synechocystis* 6803 [56-59]. The D1-V185 residue is located adjacent to the cluster near three potential substrate candidates (W2, W3 and O5). It may also block or regulate the access to the open coordination site at Mn1. The D1-V185N mutation in *Synechocystis* sp. PCC 6803 slows down the release of O_2 from 1.2 ms to about 27 ms halftime at 27 °C. In addition, the rate of exchange for the slower exchangeable water substrate molecule, Ws, was increased in the S_1 and S_2 states in the D1-V185N mutant, while both Wf, the faster exchangeable water substrate molecule, and Ws exchange rates were decreased in the S_3 state in this mutant [59]. The D1-V185T mutation in *Thermosynechococcus vestitus* resulted in similar phenotype to those in the D1-V185N in *Synechocystis* sp. PCC 6803 [60] whereas in *Synechocystis* 6803 the D1-V185T mutation hardly affected the oxygen release kinetics ($t_{1/2}$ from 1.2 ms to 1.5 ms) [57].

In the D1-V185T mutant in *T. vestitus* we found that the S_2 state was mostly present in a high spin configuration [60] although a modified low spin configuration was also observed. This observation triggered us to probe the proton release in the S_1 to S_2 transition in the context of the model mentioned above where the proton released in the S_2 to S_3 transition occurs in the $S_1Tyr_Z^{\bullet} \rightarrow S_2^{HS}Tyr_Z$ transition prior to the S_2^{HS} to S_3 transition [30,36]. One of the problem here is that measuring the proton release kinetics by using a dye as we did in [60] required an extensive washing of the PSII samples to remove all the buffers, a treatment that has deleterious effects on the particularly fragile D1-V185T mutant. In so doing, we observed a rapid phase of proton release into the bulk, the kinetics of which was close, and difficult to distinguish, to that observed following oxidation of Tyr_Z at pH 6.3 in Mn-depleted PSII. To avoid this problem, we therefore repeated the experiment here by measuring the electrochromic band shifts induced by each of the flashes in a sequence [36,54] that is an alternative way to follow the protons movements.

As the μs components kinetics in the P_{680}^+ reduction reflect the progressive increase in the equilibrium constant between $P_{680}^{+\bullet}Tyr_Z$ and $P_{680}Tyr_Z^{\bullet}$ resulting from slower proton

release/movements [61-63], we also measured the $P_{680}^{+\bullet}$ decay in the D1-V185T mutant in *T. vestitus*.

Recently [59], it was reported that the high spin EPR signal in the S_2 state of the D1-V185N PSII in *Synechocystis* 6803 was not detectable. We report here, in an independent EPR experiment, that the S_2^{HS} EPR signal in the D1-V185N PSII from *Synechocystis* 6803 is clearly present.

Materials and methods

Purification of the D1-V185N mutant from *Synechocystis 6803* was previously described in [56]. The D1 protein is PsbA2 in this mutant strain. Purification of the D1-V185T mutant from *T. vestitus* was previously described in [60]. The D1-V185T mutant has been constructed in the $psbA_3$ gene so that the wild type PSII is that one with PsbA3.

Time-resolved absorption changes measurements were performed with a lab-built spectrophotometer [64] slightly modified as described in detail in [65]. For the ΔI/I measurements the samples were diluted in 1 M betaine, 15 mM CaCl2, 15 mM MgCl2, and 40 mM MES (pH 6.5). PSII samples were dark-adapted for ~1 h at room temperature (20–22 °C) before the addition of 0.1 mM phenyl *p*–benzoquinone (PPBQ) dissolved in dimethyl sulfoxide. The chlorophyll concentration of all the samples was ~ 25 μg of Chl mL^{-1}. After the measurements, the ΔI/I values were normalized to exactly *A*673 = 1.75, that is very close to 25 μg Chl mL^{-1}. The measurements with the dye bromocresol purple were done as previously reported [36].

X-band cw-EPR spectra were recorded with a Bruker Elexsys 500 X-band spectrometer equipped with a standard ER 4102 (Bruker) X-band resonator, a Bruker teslameter, an Oxford Instruments cryostat (ESR 900) and an Oxford ITC504 temperature controller. All the samples, at ~ 1.35 mg Chl mL^{-1}, were dark-adapted for 1 h on ice then the samples were frozen in the dark (without any addition) to 198 K in a dry-ice/ethanol bath and then transferred into liquid N_2 (77 K). Prior to recording the spectra, the samples were degassed at 198 K. The S_2 state was induced by illumination with an 800 W tungsten lamp filtered by water and infrared cut-off filters for approximately 5–10 s at 198 K in a non□silvered Dewar in ethanol cooled with dry ice.

Results

Since the interpretation of the data strongly depends on the presence of an S_2^{HS} state in the D1-V185N mutant in *Synechocystis* 6803, something that was contested in [59], we will firstly show the EPR spectra recorded in this strain. Fig. 1 compares the spectra in the PSII from *Synechocystis* 6803 WT (Panel A), and D1-V185N (Panel B). The black spectra were recorded in the dark-adapted samples, the red spectra after a continuous illumination at 198 K for 5-10 s. The blue spectra are the light-*minus*-dark difference spectra.

In the WT sample (Panel A) the light-induced state exhibits a normal S_2^{LS} multiline signal similar to that induced in plant PSII and cyanobacterial PSII [10]. In contrast, in the D1-V185N PSII (Panel B), the shape and the amplitude of the multiline signal differs significantly from that one in the WT PSII. The S_2 multiline signal in the V185N sample is very similar, if not identical, to the S_2 multiline signal in the D1-V185T mutant in *T. vestitus* [60]. Importantly, a large S_2^{HS} EPR signal, centered at ~ 1700 gauss, was induced by the illumination at 198 K in the D1-V185N mutant. This S_2^{HS} EPR signal is also similar, if not identical, to the S_2^{HS} EPR signal detected in the D1-V185T mutant in *T. vestitus* [60].

In the black and red spectra, the g_z and g_y of Cytc_{550} are detected at ~ 2300 and ~ 3000 gauss, respectively. The two small negative signals in the blue spectra, between ~ 800 and ~ 1000 gauss, correspond to the negative non-heme iron signal. This means that the non-heme iron was oxidized in a proportion of centers in the dark-adapted state and reduced by the Q_A^- formed by the illumination at 198 K [66]. The large narrow signal at around 1600 gauss is due to junk Fe^{3+}. In both samples, the g = 1.9 form of the $Q_A^-Fe^{2+}Q_B$ signal (~ 3700 gauss) and the $Q_A^-Fe^{2+}Q_B^-$ signal at g = 1.6 (~ 4400 gauss) are detected. The change in their relative proportion is likely due to a different proportion of the $Q_AFe^{2+}Q_B^-$ state in the dark-adapted samples. In the black spectra, the $Q_AFe^{2+}Q_B^-$ signal is possibly present at ~ 4200 gauss and indeed larger in the mutant, *i.e.* [67].

In conclusion, from the EPR spectra in the S_2 state, there is no doubt that in the D1-V185N PSII from *Synechocystis* 6803, a S_2^{HS} EPR signal, similar to that in the D1-V185T PSII mutant from *T. vestitus* mutant [60], is formed.

Knowing with certainty that both mutants exhibit a S_2^{HS} state at pH 6.5, the question about a proton release into the bulk in the S_1 to a S_2 state with such S_2^{HS} EPR properties deserves to be again addressed.

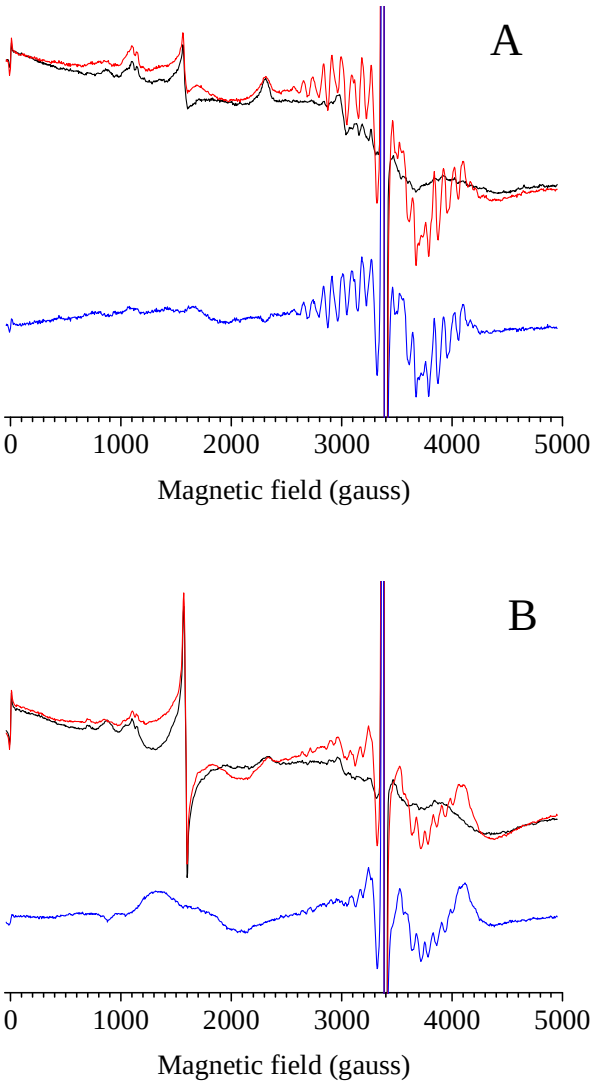

Figure 1: EPR spectra recorded at 8.6 K in WT PSII from Synechocystis 6803 (Panel A) and D1-V185N PSII from Synechocystis 6803 (Panel B). The black spectra were recorded in dark-adapted PSII. The red spectra were recorded after an illumination at 198 k for 5-10 s. The blue spectra are the "light"-minus-"dark" difference spectra. Instrument settings: [Chl] ~ 1.35 mg /ml; modulation amplitude, 25 G; microwave power, 20 mW; microwave frequency, 9.4 GHz; modulation frequency, 100 kHz. The unresolved spectral region at g ~ 2 (~ 3390 gauss) corresponds to the saturated signal from $Tyr_D^{\bullet}$.

A way to follow the change(s) of the charge(s) in and around the Mn_4CaO_5 cluster is to record the electrochromic band-shifts in the Soret region of the P_{D1} absorption spectrum at 440 nm. This measurement takes into account both the proton uptake/release and the electron transfer events, *e.g.* [54,68] and references therein. In addition, unlike the situation with the

dyes, the electrochromism is not contaminated by the protonation/deprotonation events coupled to the reduction/oxidation of the non-heme iron. For the removal of the contributions due to the reduction of Q_A the ΔI/I at 424 nm was also measured. Indeed, the electrochromism due to Q_A^- equally contributes at 440 nm and 424 nm [68]. These measurements are compared to the proton uptake/release kinetics again measured with bromocresol purple as in [60].

Panels A and B in Fig. 2 shows the absorbance changes of bromocresol purple in PsbA3-PSII and PsbA3-V185T PSII, respectively, both from *T. vestitus*. An uptake of proton by PSII induces an increase in the ΔI/I at 575 nm and a release of proton into the bulk by PSII induces a decrease of the ΔI/I. After the first flash (black points), in both samples, there was a large increase in the absorption. This increase is due to the proton uptake following the reduction of the non-heme iron [36]. In PsbA3-PSII (Panel A) there is no detectable proton release associated to the S_1 to S_2 transition, see a full analysis of a similar experiment in [36]. In the PsbA3-V185T mutant, in contrast with the previous report [60], the decrease in the ΔI/I in the 10 µs to 100 µs time range is very small suggesting that a proton release, if any, occurs in a very low proportion of the centers. This lack of proton release is very likely due to the use of a PsbA3-V185T PSII sample less damaged by the washing steps than in our previous report [60]. The proton uptake is detected after each flash as previously reported [36] that explains the drift (not subtracted in Panels A and B) observed on each flash. The proton release kinetics in the PsbA3-V185T PSII in the S_2 to S_3 transition (red points) and in the S_0 to S_1 transition (green points) appears hardly affected when compared to PSbA3-PSII. The release of the first proton in the S_3 to S_0 transition is also hardly affected in the mutant. In contrast, the release of the second proton is strongly slowed down with a kinetics similar to the O_2 release (~ 20-30 ms) [56,60].

Panel C in Fig.2 shows the kinetics of the 440 nm-*minus*-424 nm difference in the PsbA3-V185T PSII from *T. vestitus*. The results can be compared to those obtained in PsbA3-PSII that have been described in details previously [36,54]. After the first flash (black points), the kinetics that corresponds to the $S_1Tyr_Z^\bullet$ to the S_2Tyr_Z transition is slightly slowed down from 10-20 µs to 50-60 µs in the PsbA3-V185T mutant. After the second flash (red points) the kinetics is biphasic with a fast phase ($t_{1/2}$ ~ 10-15 µs) that we have attributed to a proton movement coupled to the $S_2^{LS}Tyr_Z^\bullet$ to $S_2^{HS}Tyr_Z^\bullet$ transition. The slow phase was attributed to the $S_2^{HS}Tyr_Z^\bullet$ to the S_3Tyr_Z transition. In the PsbA3-V185T mutant the two phases are not really differentiated that makes the interpretation difficult even if this result could suggest a slowing done of the proton release in the S_2 to S_3 transition. In the PsbA3-PSII, after the fourth flash, the kinetics is also biphasic with the fast phase corresponding to the electron

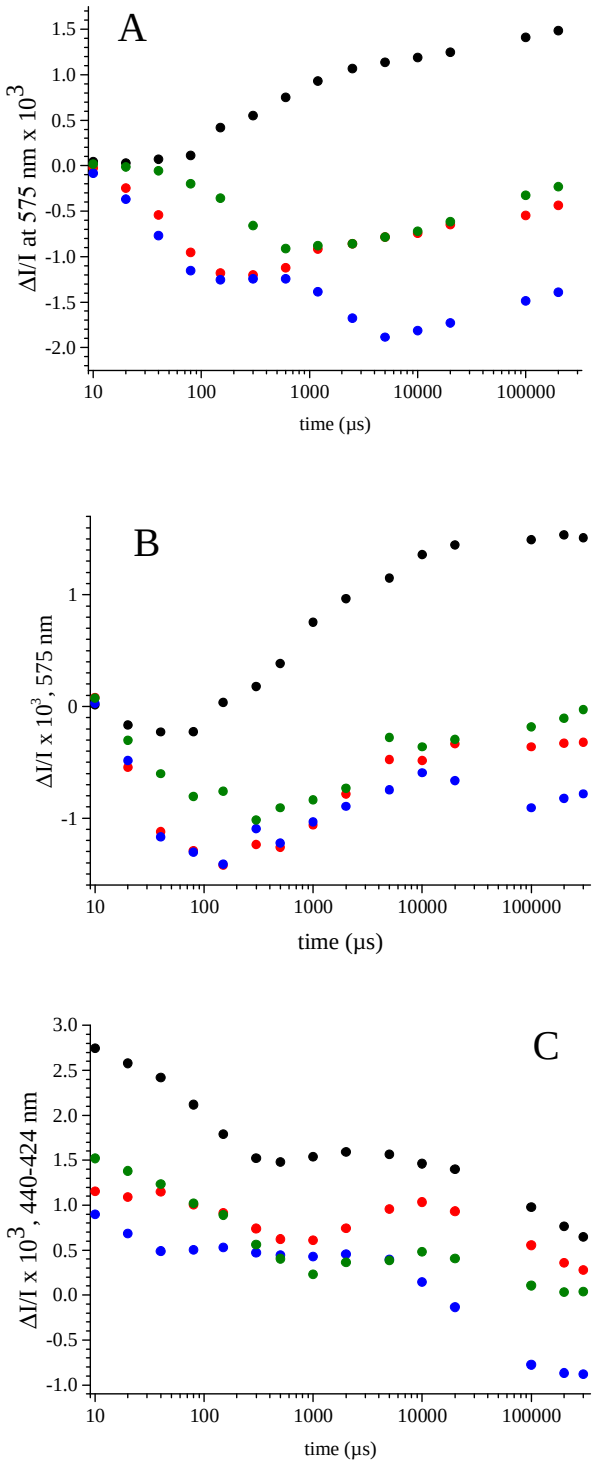

Figure 2: Time-courses of the absorption changes of bromocresol purple at 575 nm in PsbA3-PSII (Panel A) and PsbA3-V185T PSII (Panel B) after the 1st flash (black points), the 2nd flash (red points), the 3rd flash (blue points), and the 4th flash (green points). Panel C; time-courses of the absorption change differences 440 nm-minus-424 nm after the first flash (black), the second flash (red), the third flash (blue), and the fourth flash (green) given to dark-adapted PsbA3-V185T PSII in the presence of 100 µM PPBQ with flashes spaced 400 ms apart.

transfer in the S_0 to S_1 transition ($t_{1/2}$ ~ 10-15 µs), which precedes the proton release with a $t_{1/2}$ ~ 200 µs [36,54]. In the PsbA3-V185T, after the fourth flash (green points), although the two phases are also difficult to be detected due to a less good signal-to-noise ratio, and an increase miss parameter (see however below), the two phases seem to have more or less the same kinetics. The big difference between Panel A and Panel B is the slow phase after the third flash (blue points) with a $t_{1/2}$ ~ 20-30 ms in D1-V185T PSII, which is similar to that of the proton release in this sample. After the 4th flash the slow decay certainly originates from a residual S_3 to S_0 transition due to the misses but we have no clear explanation for the slow drift after the 1st and 2nd flash since the redox events at the non-heme iron do not contribute in the electrochromism of P_{D1}.

Each event, such as a change in the kinetics of electron and proton motion, should affect the$P_{680}^{+\bullet}Tyr_Z \leftrightarrow P_{680}Tyr_Z^{\bullet}$ equilibrium and therefore the $P_{680}^{+\bullet}$ decay kinetics. Panels A, B, C, and D in Fig. 3 show the kinetics of flash-induced absorption changes measured at 432 nm in PsbA3 PSII (black), and PsbA3-V185T PSII (red) after the 1st flash (Panel A), the 2nd flash (Panel B), the 3rd flash (Panel C) and the 4th flash (Panel D). In all the S_n states, the decay of P_{680}^{+} in the D1-V185T mutant is significantly slower both in the ns time-domain corresponding to the pure electron transfer step, and the µs time-domain where the electron transfer(s) is(are) coupled to proton movements. The $P_{680}^{+\bullet}Tyr_Z \leftrightarrow P_{680}Tyr_Z^{\bullet}$ is therefore shifted to the left in the PsbA3-V185T mutant in all the S_n states [61,63] and we expect that some of the proton movements coupled to the electron transfer are also slowed down.

Panel E in Fig. 3 shows the ΔI/I measured 20 ns after each flash of the sequence in the PsbA3 PSII (black) and in the PsbA3-V185T PSII (red). Due to the slower decay of P_{680}^{+} in the S_2 and S_3 states [69] than in the S_0 and S_1 states we obtain an oscillation with the period of four. Since in PsbA3 PSII the decay of $P_{680}^{+\bullet}$ is faster in all the S_n states than in the PsbA3-V185T PSII, the ΔI/I values in PsbA3 PSII 20 ns after the flashes are smaller in all the Sn states. However, the oscillations are similar in both samples, which indicates that in the PsbA3-V185T PSII used here the miss parameter is not much larger than in the PsbA3 PSII.

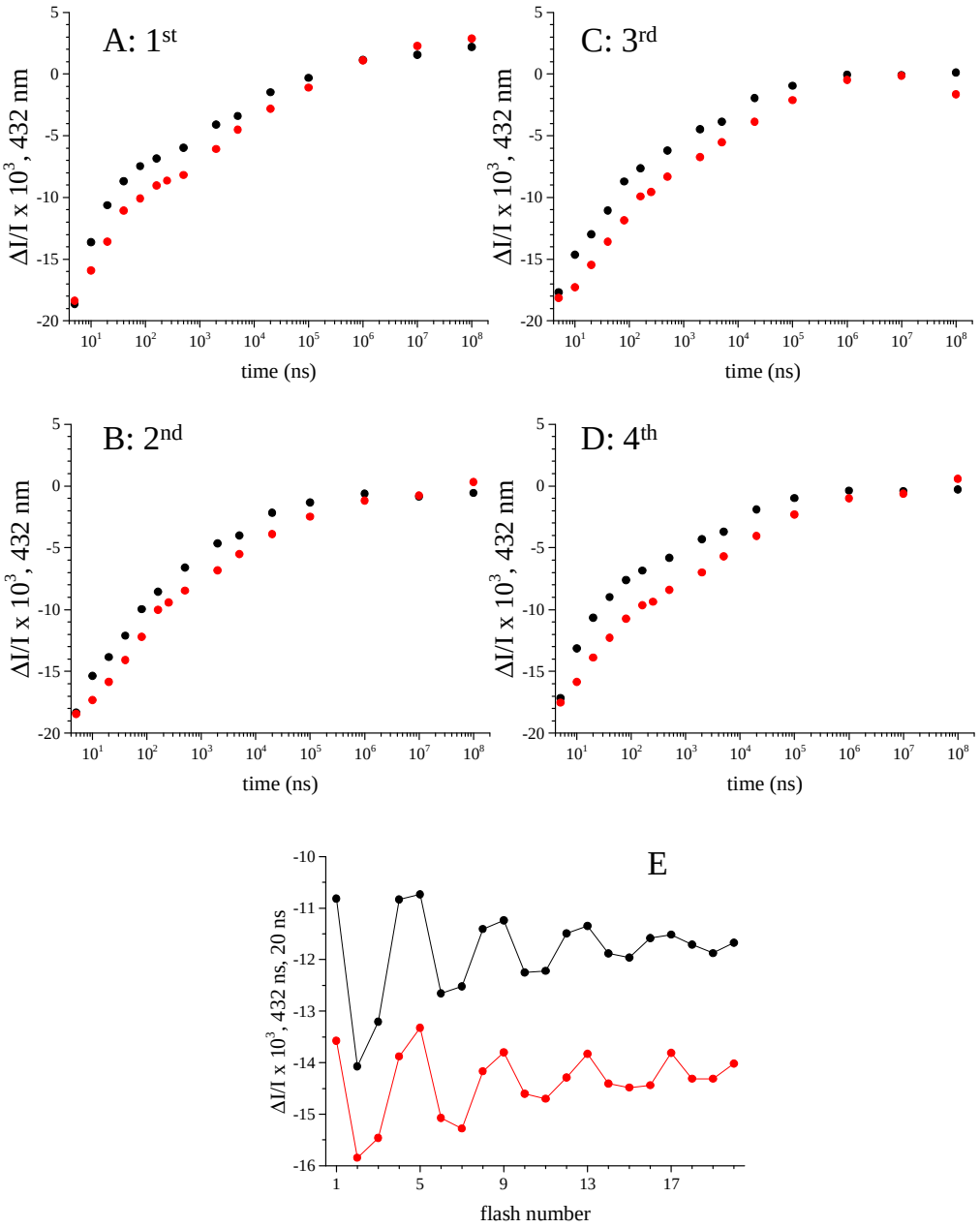

Figure 3: Kinetics of flash-induced absorption changes measured at 432 nm in PsbA3 PSII (black), and PsbA3-V185T PSII (red) after the 1st flash (Panel A), the 2nd flash (Panel B), the 3rd flash (Panel C) and the 4th flash (Panel D). The amplitudes of the kinetics were normalized to OD673nm = 1.75 (a Chl concentration of ~ 25 μg/ml). 100 μM PPBQ was added before the measurements were taken. Panel E shows the amplitude of the ΔI/I at 20 ns after each flash of the sequence with flashes spaced 400 ms apart.

Discussion

One of the main results shown in this work is the presence of a S_2^{HS} in the D1-V185N PSII from *Synechocystis* 6803 that exhibits EPR characteristics very similar to those in the D1-V185T PSII mutant from *T. vestitus* [60]. The discrepancy between the conclusion made here and that in [59] is very likely due to the base lines which are too strongly distorted in the low field region in [59], mainly in the wild type, to make the S_2^{HS} EPR signal easily distinguishable (that is nevertheless clearly present).

It has been shown that the equilibrium between the S_2^{LS} and S_2^{HS} states is pH dependent [30], with a p*K*a ~ 8.3 for the native Mn_4CaO_5 cluster and a p*K*a corrected to ~ 7.0 for the Mn_4SrO_5 cluster [36]. In addition, these S_2^{HS} state formed by the room temperature flash illumination were able to progress to S_3 under a further continuous illumination at 198 K. The low p*K*a value in PSII with a Mn_4SrO_5 cluster explains why the S_2^{HS} to S_3 transition may occur in a significant proportion of centers at pH 6.5. Since the PsbA3-V185T PSII exhibited also a large proportion of centers with a S_2^{HS} signal at pH 6.5 we could expect that these centers were able to progress to S_3 at 198 K. In PsbA3-V185T PSII with a Mn_4CaO_5 cluster (spectrum *a* in figure 9 in [60]) this was not so evident. In contrast, in PsbA3-V185T PSII with a Mn_4SrO_5 cluster, the effect of the 198 K illumination was more pronounced (spectrum *b* in figure 9 in [60]). However, the S_2^{HS} EPR signal that disappeared in PsbA3-V185T PSII with a Mn_4SrO_5 cluster upon the 198 K illumination had a shape similar to that in PsbA3 PSII (with both Ca and Sr in the cluster). This observation suggests some heterogeneity in the EPR properties of the S_2^{HS} state in PsbA3-V185T PSII with a Mn_4SrO_5 cluster. Importantly, since the illumination at 198 K results in the formation of the S_2^{HS} and S_2^{LS} states in both species, it seems likely that each of these two states arises from two structurally different S_1 states.

The previously mentioned possibility [60] for a S_2^{HS} to S_3 transition occurring at 198 K in PsbA3-V185T PSII seemed to be supported by the detection of a proton release on the first flash, see [36]. However, it is shown here that this proton release does not occurs in active PSII but rather as originating from the oxidation of Tyr_Z in a minor sub-population Mn depleted centers in the PsbA3-V185T sample used for proton release experiment in [60]. In conclusion, the S_2^{HS} state in PsbA3-V185T PSII, with EPR properties different from those in PsbA3-PSII, is very likely unable to progress to S_3 at 198 K.

The S_2^{HS} EPR signal in the D1-V185T PSII from *T. vestitus*, and the D1-V185N PSII from *Synechocystis* 6803, have a shape very similar to that of the spectrum induced by near-

infrared illumination of the S_2^{HS} state at high pH in PsbA3-PSII see figure 3 in [70]. Presently, there is no explanation of the near-infrared illumination however this similarity could suggest that the two states have a Mn_4CaO_5 cluster with similar structural characteristics.

The inability of the S_2^{HS} state in D1-V185T PSII to progress to S_3 at 198 K, as discussed, may arise from alterations in the protonation state, possibly influenced by changes in the hydrogen-bonding network around the Mn_4CaO_5 cluster. This possibility is reinforced by the EPR signal similarities observed between D1-V185T and D1-V185N mutants, which suggest structural differences are subtle but functionally significant. The comparison of these states to the Mn_4CaO_5 cluster under near-infrared illumination at high pH in PsbA3-PSII, where small structural changes were proposed, hints that the proton transfer dynamics may be a critical factor influenced by these mutations.

Functionally significant hydrogen bonding changes due to mutations at D1-V185 likely affect the stabilization and dynamics of substrate water molecules in the S_3 state based upon previous findings [56,58,59]. The slowdowns of both the lag and oxygen release phase during the S_3-S_0 transition have been attributed to changes in the H-bond network that corresponds to a suboptimal configuration of reactants and an associated entropic penalty to cross the activation barrier of the transition state [56]. The observation of slower water exchange in S_3 [59] has been suggested to be the result of the stabilization of water molecules due to altered hydrogen-bonding around the inserted substrate water, O6, although the mechanism of substrate exchange remains to be elucidated. The D1-V185T and D1-V185N mutations replace the non-polar valine side chain with threonine or asparagine, which can introduce non-native hydrogen bonds to the putative O6 substrate and with nearby water molecules, thereby affecting both water binding and proton release. In the S_2 state, prior to the insertion of the O6 substrate on Mn1, waters in the vicinity of D1-V185 would also be affected by the introduction of non-native H-bonding due to the mutations. This aligns with the broader idea that the D1-V185 mutations impact the coordination and movement of substrate waters, reflecting a complex interplay between proton transfer, hydrogen bonding, and the structural integrity of the water-splitting machinery in PSII.

In this context, the slower water exchange in S_3 may thus not solely results from stronger binding of water molecules but also from impaired proton transfer dynamics, both of which are sensitive to the specific hydrogen-bonding interactions introduced by the D1-V185 mutations. Although, more further experimental tests will be essential, this hypothesis is consistent with the observed spectroscopic and proton release data, suggesting that the

mutations perturb the fine balance of water and proton dynamics essential for efficient oxygen evolution.

One of the most intriguing observations of this study is that in the release of the 2 protons during the S_3-to-S_0 transition in the D1-V185 mutants, it is the second of the two protons released during this transition that is affected, whereas the first proton release, which occurs rapidly following the formation of $Tyr_Z^{\bullet}$, remains largely unaffected. This initial fast proton release is proposed to be linked to the electrostatic impact of uncompensated charge formation upon effects of formation of Tyr_ZOH-His190 → $Tyr_ZO^{\bullet}$-H^+His190 [71,72]. Functionally, this is proposed to occur to prepare D1-Asp61 as a proton acceptor for the slower, second proton release from substrate water O6 [71-74]. The transient electric field during the $Tyr_ZO^{\bullet}$-H^+His190 state is calculated to promote proton transfer from W1 to Asp61, inducing rearrangements in the cluster of residues D1-Asp61, D1-Glu65, and D2-Glu312 into a configuration that facilitates rapid proton egress to the bulk [71-73]. The rapid exit of this proton is likely gated, preventing back-reactions, *e.g.* [15,16]. Once deprotonated, the cluster forms the base that accepts the proton from substrate water O6, facilitating the final electron transfer leading to O_2 formation [74]. The fact that the fast proton release remains unaffected by the mutation, while the second proton release is delayed, is consistent with the D1-V185 residue being distant from the fast proton release vector but positioned near the substrate water (O6), where deprotonation occurs. Thus, the delayed second proton release in the mutants is attributed to the disruption of the hydrogen-bonding network around O6, which slows the proton transfer pathway necessary for its deprotonation and the final stages of water oxidation.

Acknowledgements

This work has been in part supported by (i) the French Infrastructure for Integrated Structural Biology (FRISBI) ANR-10-INBS-05, (ii) the Labex Dynamo (ANR-11-LABX-0011-01) and (iii) the JSPS-KAKENHI Grant in Scientific Research on Innovative Areas JP17H064351 and a JSPS-KAKENHI Grant 21H02447. One of the PSII preparations used in this work was done by T. Tibiletti.

References

[1] D. Shevela, J.F. Kern, G. Govindjee, J. Messinger, Solar energy conversion by photosystem II: principles and structures, Photosynth. Res. 156 (2023) 279-307. https://doi.org/10.1007/s11120-022-00991-y

[2] Y. Umena, K. Kawakami, J.-R. Shen, N. Kamiya, Crystal structure of oxygen evolving Photosystem II at a resolution of 1.9 angstrom, Nature 473 (2011) 55–60. https://doi.org/10.1038/nature09913

[3] H. Ago, H. Adachi, Y. Umena, T. Tashiro, K. Kawakami, N. Kamiya, L.R. Tian, G.Y. Han, T.Y. Kuang, Z.Y. Liu, F.J. Wang, H.F. Zou, I. Enami, M. Miyano, J.-R. Shen, Novel features of eukaryotic photosystem II revealed by its crystal structure analysis from a red alga, J. Biol. Chem. 291 (2016) 5676–5687. https://doi.org/10.1074/jbc.M115.711689

[4] C.J. Gisriel, J. Wang, J. Liu, D.A. Flesher, K.M. Reiss, H.-L. Huang, K.R. Yang, W.H. Armstrong, M.R. Gunner, V.S. Batista, R.J. Debus, G.W. Brudvig, High resolution cryo-electron microscopy structure of photosystem II from the mesophilic cyanobacterium, *Synechocystis* sp. PCC 6803, Proc. Natl. Acad. Sci. U. S. A. 119 (2022), e2116765118. https://doi.org/10.1073/pnas.2116765118

[5] A.R. Holzwarth, M.G. Müller, M. Reus, M. Nowaczyk, J. Sander, M. Rögner, Kinetics and mechanism of electron transfer in intact Photosystem II and in the isolated reaction center: pheophytin is the primary electron acceptor, Proc. Natl. Acad. Sci. U. S. A. 103 (2006) 6895–6900. https://doi.org/10.1073/pnas.0505371103

[6] F. Muh, M. Plockinger, T. Renger, Electrostatic asymmetry in the reaction center of Photosystem II, J. Phys. Chem. Lett. 8 (2017) 850–858. https://doi.org/10.1021/acs.jpclett.6b02823

[7] A. Sirohiwal, D.A. Pantazis, Reaction center excitation in Photosystem II: From multiscale modeling to functional principles, Acc. Chem. Res. 56 (2023) 2921−2932. https://doi.org/10.1021/acs.accounts.3c00392

[8] D.J. Vinyard, G.M. Ananyev, G.C. Dismukes, Photosystem II: the reaction center of oxygenic photosynthesis, Annu. Rev. Biochem. 82 (2013) 577–606. https://10.1146/annurev-biochem-070511-100425

[9] J. Yano, J. Kern, V.K. Yachandra, Structure function studies of Photosystem II using X-ray free electron lasers, Annu. Rev. Biophys. 53 (2024)343–65. https://doi.org/10.1146/annurev-biophys-071723-102519

[10] W. Lubitz D.A. Pantazis N. Cox , Water oxidation in oxygenic photosynthesis studied by magnetic resonance techniques, FEBS Lett. 597 (2023) 6–29. https://doi.org/10.1002/1873-3468.14543

[11] N. Oliver, A.P. Avramov, D.J. Nürnberg, H. Dau, R.L. Burnap, From manganese oxidation to water oxidation: assembly and evolution of the water-splitting complex in photosystem II, Photosynth. Res. 152 (2022) 107–133. https://doi.org/10.1007/s11120-022-00912-z

[12] T. Oliver, T.D. Kim, J.P. Trinugroho, V. Cord´on-Preciado, N. Wijayatilake, A. Bhatia, A.W. Rutherford, T. Cardona, The evolution and evolvability of photosystem II, Annu. Rev. Plant Biol. 74 (2023) 24.1–24.33, https://doi.org/10.1146/annurev-arplant-070522-062509

[13] P. Joliot, Period-four oscillations of the flash-induced oxygen formation in photosynthesis, Photosynth. Res. 76 (2003) 65–72. https://doi.org/10.1023/A:1024946610564

[14] B. Kok, B. Forbush, M. McGloin, Cooperation of charges in photosynthetic O_2 evolution–I. A linear four step mechanism, Photochem. Photobiol. 11 (1970) 457–475. https://doi.org/10.1111/j.1751-1097.1970.tb06017.x

[15] J. Kern, R. Chatterjee, I.D. Young, F.D. Fuller, L. Lassalle, M. Ibrahim, S. Gul, T. Fransson, A.S. Brewster, R. Alonso-Mori, R. Hussein, M. Zhang, L. Douthit, C. de Lichtenberg, M. Hon Cheah, D. Shevela, J. Wersig, I. Seuffert, D. Sokaras, E. Pastor, C. Weninger, T. Kroll, R.G. Sierra, P. Aller, A. Butryn, A.M. Orville, M. Liang, A. Batyuk, J.E. Koglin, S. Carbajo, S. Boutet, N.W. Moriarty, J.M. Holton, H. Dobbek, P.D. Adams, U. Bergmann, N.K. Sauter, A. Zouni, J. Messinger, J. Yano, V.K. Yachandra, Structures of the intermediates of Kok's photosynthetic water oxidation clock, Nature 563 (2018) 421. https://doi.org/10.1038/s41586-018-0681-2

[16] A. Bhowmick, P.S. Simon, I. Bogacz, R. Hussein, M. Zhang, H. Makita, M. Ibrahim, R. Chatterjee, M.D. Doyle, M. Hon Cheah, P. Chernev, F.D. Fuller, T. Fransson, R. Alonso-Mori, A.S. Brewster, N.K. Sauter, U. Bergmann, H. Dobbek, A. Zouni, J. Messinger, J. Kern, V.K. Yachandra, J. Yano, Going around the Kok cycle of the water oxidation reaction with femtosecond X-ray crystallography, IUCrJ 10 (2023) 642–655. https://doi.org/10.1107/S2052252523008928

[17] H. Li, Y. Nakajima, E. Nango, S. Owada, D. Yamada, K. Hashimoto, F. Luo, R. Tanaka, F. Akita, K. Kato, J. Kang, Y. Saitoh, S. Kishi, H. Yu, N. Matsubara, H. Fujii, M. Sugahara, M. Suzuki, T. Masuda, T. Kimura, T. Nguyen Thao, S. Yonekura, L-J. Yu, T. Tosha, K. Tono, Y. Joti, T. Hatsui, M. Yabashi, M. Kubo, S. Iwata, H. Isobe, K. Yamaguchi, M. Suga, J-R. Shen,

Oxygen-evolving photosystem II structures during S1–S2–S3 transitions, Nature 626 (2024) 670–677. https://doi.org/10.1038/s41586-023-06987-5

[18] C. de Lichtenberg, L. Rapatskiy, M. Reus, E. Heyno, A. Schnegg, M.M. Nowaczyk, W. Lubitz, J. Messinger, N. Cox, Assignment of the slowly exchanging substrate water of nature's water-splitting cofactor, Proc. Natl. Acad. Sci. U. S. A. 121 (2024) e2319374121. https://doi.org/10.1073/pnas.2319374121

[19] S.L. Dexheimer, M.P. Klein, Detection of a paramagnetic intermediate in the S_1 state of the photosynthetic oxygen-evolving complex, J. Am. Chem. Soc. 114 (1992) 2821–2826. https://doi.org/10.1021/ja00034a010

[20] T. Yamauchi, H. Mino, T. Matsukawa, A. Kawamori, T.-A. Ono, Parallel polarization electron paramagnetic resonance studies of the S_1-state manganese cluster in the photosynthetic oxygen-evolving system, Biochemistry 36 (1997) 7520–7526. https://doi.org/10.1021/bi962791g

[21] K.A. Campbell, J.M. Peloquin, D.P. Pham, R.J. Debus, R.D. Britt, Parallel polarization EPR detection of an S1-State "Multiline" EPR signal in Photosystem II particles from *Synechocystis* sp. PCC 6803, J. Am. Chem. Soc. 120 (1998) 447–448. https://doi.org/10.1021/ja972693y

[22] M. Drosou, G. Zahariou, D.A. Pantazis, Orientational Jahn-Teller isomerism in the dark-stable state of nature's water oxidase, Angew. Chem. Int. Ed. 60 (2021,13493–13499. https://doi.org/10.1002/anie.202103425

[23] G.C. Dismukes, Y. Siderer, Intermediates of a polynuclear manganese center involved in photosynthetic oxidation of water, Proc. Natl. Acad. Sci. U. S. A. 78 (1981) 274–278. https://doi.org/10.1073/pnas.78.1.274

[24] J.M. Peloquin, K.A. Campbell, D.W. Randall, M.A. Evanchik, V.L. Pecoraro, W. H. Armstrong, R.D. Britt, Mn-55 ENDOR of the S2-state multiline EPR signal of photosystem II: implications on the structure of the tetranuclear mn cluster, J. Am. Chem. Soc. 122 (2000) 10926–10942. https://doi.org/10.1021/ja002104f

[25] N. Cox, L. Rapatskiy, J.-H. Su, D.A. Pantazis, M. Sugiura, L. Kulik, P. Dorlet, A.W. Rutherford, F. Neese, A. Boussac, W. Lubitz, J. Messinger, Effect of Ca^{2+}/Sr^{2+} substitution on the electronic structure of the oxygen-evolving complex of photosystem II: a combined multifrequency EPR, mn-55-ENDOR, and DFT study of the S_2 state, J. Am. Chem. Soc. 133 (2011) 3635–3648. https://doi.org/10.1021/ja110145v

[26] J.-L. Zimmermann, A.W. Rutherford, Electron paramagnetic resonance studies of the oxygen-evolving enzyme of photosystem II, Biochim. Biophys. Acta 767 (1984) 160–167, https://doi.org/10.1016/0005-2728(84)90091-4

[27] J.L. Casey, K. Sauer, Electron paramagnetic resonance detection of a cryogenically photogenerated intermediate in photosynthetic oxygen evolution, Biochim. Biophys. Acta 767 (1984) 21–28. https://doi.org/10.1016/0005-2728(84)90075-6

[28] A. Boussac, S. Un, O. Horner, A.W. Rutherford, High spin states ($S \geq 5/2$) of the photosystem II manganese complex, Biochemistry 37 (1998) 4001–4007. https://doi.org/10.1021/bi9728710

[29] A. Boussac, H. Kuhl, S. Un, M. Rögner, A.W. Rutherford, Effect of near-infrared light on the S_2-state of the manganese complex of photosystem II from *Synechococcus elongatus*, Biochemistry 37 (1998) 8995–9000, https://doi.org/10.1021/bi980195b

[30] A. Boussac, I. Ugur, A. Marion, M. Sugiura, V.R.I. Kaila, A.W. Rutherford, The low spin - high spin equilibrium in the S_2-state of the water oxidizing enzyme, Biochim. Biophys. Acta 2018 (1859) 342–356. https://doi.org/10.1016/j. bbabio.2018.02.010.

[31] A. Boussac, Temperature dependence of the high-spin S_2 to S_3 transition in photosystem II: mechanistic consequences, Biochim. Biophys. Acta 2019 (1860) 508–518. https://doi.org/10.1016/j.bbabio.2019.05.001

[32] D.A. Pantazis, W. Ames, N. Cox, W. Lubitz, F. Neese, Two interconvertible structures that explain the spectroscopic properties of the oxygen-evolving complex of photosystem II in the S_2 state, Angew. Chem. Intl. Ed. 51 (2012) 9935–9940. https://doi.org/10.1002/anie.201204705

[33] T.A. Corry, P.J. O'Malley, Proton isomers rationalize the high- and low-spin forms of the S2 state intermediate in the water-oxidizing reaction of photosystem II, J. Phys. Chem. Lett. 10 (2019) 5226–5230. https://doi.org/10.1021/acs. jpclett.9b01372

[34] T.A. Corry, P.J. O'Malley, Molecular identification of a high-spin deprotonated intermediate during the S_2 to S_3 transition of nature's water-oxidizing complex, J. Am. Chem. Soc. 142 (2020) 10240–10243. https://doi.org/10.1021/jacs.0c01351

[35] M. Barchenko, P.J. O'Malley, A reappraisal of the S_2 state of nature's water oxidizing complex in its low and high spin forms, J. Phys. Chem. Lett. 15 (2024) 5883−5886. https://doi.org/10.1021/acs.jpclett.4c00997

[36] A. Boussac, M. Sugiura, J. Sellés, Probing the proton release by Photosystem II in the S_1 to S_2 high-spin transition, Biochim. Biophys. Acta 1863 (2022), 148546. https://doi.org/10.1016/j.bbabio.2022.148546

[37] Y. Sanakis, J. Sarrou, G. Zahariou, V. Petrouleas, Q-band electron paramagnetic resonance studies of the S_3 state of the OEC of Photosystem II, in: J.F. Allen, E. Gantt, J.H. Golbeck, B. Osmond (Eds.), Photosynthesis. Energy From the Sun, Springer, Dordrecht, 2008. https://doi.org/10.1007/978-1-4020-6709-9_108

[38] A. Boussac, M. Sugiura, A.W. Rutherford, P. Dorlet, Complete EPR spectrum of the S_3-state of the oxygen-evolving photosystem II, J. Am. Chem. Soc. 131 (2009) 5050–5051. https://doi.org/10.1021/ja900680t

[39] N. Cox, M. Retegan, F. Neese, D.A. Pantazis, A. Boussac, W. Lubitz, Electronic structure of the oxygen evolving complex in photosystem II prior to O-O bond formation, Science 345 (2014) 804–808. https://doi.org/10.1126/science.1254910

[40] A. Boussac, A.W. Rutherford, M. Sugiura, Electron transfer pathways from the S_2-states to the S_3-states either after a Ca^{2+}/Sr^{2+} or a Cl^-/I^- exchange in Photosystem II from *Thermosynechococcus elongatus*, Biochim. Biophys. Acta 1847 (2015) 576–586. http://dx.doi.org/10.1016/j.bbabio.2015.03.006

[41] D.A. Marchiori, R.J. Debus, R.D. Britt, Pulse EPR spectroscopic characterization of the S_3 state of the oxygen-evolving complex of photosystem II isolated from *Synechocystis*, Biochemistry 59 (2020) 4864–4872. https://doi.org/10.1021/acs.biochem.0c00880

[42] G. Zahariou, N. Ioannidis, Y. Sanakis, D.A. Pantazis, Arrested substrate binding resolves catalytic intermediates in higher-plant water oxidation, Angew. Chem. Intl. Ed. 60 (2020) 3156–3162. https://doi.org/10.1002/anie.202012304

[43] M. Chrysina, E. Heyno, Y. Kutina, M. Reus, H. Nilsson, M.M. Nowaczyk, S. DeBeer, F. Neese, J. Messinger, W. Lubitz, N. Cox, Five-coordinate Mn^{IV} intermediate in the activation of nature's water splitting cofactor, Proc. Nat. Aca. Sci. USA 116 (2019) 16841–16846. https://doi.org/10.1073/pnas.1817526116

[44] K.G.V. Havelius, J.-H. Su, Y. Feyziyev, F. Mamedov, S. Styring, Spectral resolution of the split EPR signals induced by illumination at 5 K from the S_1, S_3, and S_0 states in photosystem II, Biochemistry 45 (2006) 9279–9290. https://doi.org/10.1021/bi060698e

[45] A. Boussac, M. Sugiura, T.-L. Lai, A.W. Rutherford, Low-temperature photochemistry in Photosystem II from *Thermosynechococcus elongatus* induced by visible and near-infrared light, Philos. Trans. R. Soc. London, Ser. B 363 (2008) 1203–1210. https://doi.org/10.1098/rstb.2007.2216

[46] V. Krewald, F. Neese, D.A. Pantazis, Implications of structural heterogeneity for the electronic structure of the final oxygen-evolving intermediate in photosystem II, J. Inorg. Biochem. 199 (2019), 110797. https://doi.org/10.1016/j.jinorgbio.2019.110797

[47] M. Drosou, D.A. Pantazis, Redox isomerism in the S_3 state of the oxygen-evolving complex resolved by coupled cluster theory, Chem. Eur. J. 27 (2021) 12815–12825. https://doi.org/10.1002/chem.202101567

[48] H. Isobe, M. Shoji, T. Suzuki, J.-R. Shen, Spin, valence, and structural isomerism in the S_3 state of the oxygen-evolving complex of photosystem II as a manifestation of multimetallic cooperativity, J. Chem. Theory Comput. 15 (2019) 2375–2391. https://doi.org/10.1021/acs.jctc.8b01055

[49] M. Chrysina, M. Drosou, R.G. Castillo, M. Reus, F. Neese, V. Krewald, D.A. Pantazis, S. DeBeer, Nature of S-states in the oxygen-evolving complex resolved by high-energy resolution fluorescence detected X-ray absorption spectroscopy, J. Am. Chem. Soc. 145 (2023) 25579–25594. https://doi.org/10.1021/jacs.3c06046

[50] A. Klauss, M. Haumann, H. Dau, Seven steps of alternating electron and proton transfer in photosystem II water oxidation traced by time-resolved photothermal beam deflection at improved sensitivity, J. Phys. Chem. B 119 (2015) 2677–2689. https://doi.org/10.1021/jp509069p

[51] I. Zaharieva, H. Dau, M. Haumann, Sequential and coupled proton and electron transfer events in the $S_2 \rightarrow S_3$ transition of photosynthetic water oxidation revealed by time-resolved X-ray absorption spectroscopy, Biochemistry 55 (2016) 6996–7004. https://doi.org/10.1021/acs.biochem.6b01078

[52] Y. Okamoto, Y. Shimada, R. Nagao, T. Noguchi, Proton and water transfer pathways in the $S_2 \rightarrow S_3$ transition of the water-oxidizing complex in photosystem II: time-resolved infrared analysis of the effects of D1–N298A mutation and NO_3-substitution, J. Phys. Chem. B 125 (2021) 6864–6873. https://doi.org/10.1021/acs.jpcb.1c03386

[53] S.M. Mausle, A. Abzaliyeva, P. Greife, P.S. Simon, R. Perez, Y. Zilliges, H. Dau, Activation energies for two steps in the $S_2 \rightarrow S_3$ transition of photosynthetic water oxidation from time-resolved single-frequency infrared spectroscopy, J. Chem. Phys. 153 (2020) 215101. https://doi.org/10.1063/5.0027995

[54] A. Boussac, J. Sellés, M. Sugiura, What can we still learn from the electrochromic band-shifts in photosystem II? Biochim. Biophys. Acta 1861 (2020), 148176. https://doi.org/10.1016/j.bbabio.2020.148176

[55] M. Ibrahim, T. Fransson, R. Chatterjee, M.H. Cheah, R. Hussein, L. Lassalle, K.D. Sutherlin, I.D. Young, F.D. Fuller, S. Gul, I.S. Kim, P.S. Simon, C. de Lichtenberg, P. Chernev, I. Bogacz, C.C. Pham, A.M. Orville, N. Saichek, T. Northen, A. Batyuk, S. Carbajo, R. Alonso-Mori, K. Tono, S. Owada, A. Bhowmick, R. Bolotovsky, D. Mendez, N.W.

Moriarty, J.M. Holton, H. Dobbek, A.S. Brewster, P.D. Adams, N. K. Sauter, U. Bergmann, A. Zouni, J. Messinger, J. Kern, V.K. Yachandra, J. Yano, Untangling the sequence of events during the $S_2 \rightarrow S_3$ transition in photosystem II and implications for the water oxidation mechanism, Proc. Natl. Acad. Sci. U. S. A.117 (2020) 12624–12635. https://doi.org/10.1073/pnas.2000529117

[56] H. Bao, R.L. Burnap, Structural rearrangements preceding dioxygen formation by the water oxidation complex of Photosystem II, Proc. Natl. Acad. Sci. U. S. A. 112 (2015) 6139–6147. https://doi.org/10.1073/pnas.1512008112

[57] P.L. Dilbeck, H. Bao, C.L. Neveu, R.L. Burnap, Perturbing the water cavity surrounding the manganese cluster by mutating the residue D1-Valine 185 has a strong effect on the water oxidation mechanism of Photosystem II, Biochemistry 52 (2013) 6824–6833. https://doi.org/10.1021/bi400930g

[58] C.J. Kim, H. Bao, R.L. Burnap, R.J. Debus, Impact of D1-V185 on the water molecules that facilitate O_2 formation by the catalytic Mn_4CaO_5 cluster in Photosystem II, Biochemistry 57 (2018) 4299–4311. https://doi.org/10.1021/acs.biochem.8b00630

[59] C. de Lichtenberg, A.P. Avramov, M.Q. Zhang, F. Mamedov, R.L. Burnap, J. Messinger, The D1-V185N mutation alters substrate water exchange by stabilizing alternative structures of the Mn4Ca-cluster in photosystem II, Biochim. Biophys. Acta 1862 (2021) 148319. https://doi.org/10.1016/j.bbabio.2020.148319

[60] M. Sugiura, T. Tibiletti, I. Takachi, Y. Hara, S. Kanawaku, J. Sellés, A. Boussac, Probing the role of Valine 185 of the D1 protein in the Photosystem II oxygen evolution, Biochim. Biophys. Acta 1859 (2018) 1259–1273. https://doi.org/10.1016/j.bbabio.2018.10.003

[61] M.J. Schilstra, F. Rappaport, J.H. Nugent, C.J. Barnett, D.R. Klug, Proton/hydrogen transfer affects the S state-dependent microsecond phases of P_{680}^+ reduction during water splitting, Biochemistry 37 (1998) 3974–3981. https://doi.org/10.1021/bi9713815

[62] P. Kuhn, H. Eckert, H.J. Eichler, G. Renger, Analysis of the P_{680}^+ reduction pattern and its temperature dependence in oxygen evolving PSII core complexes from a thermophilic cyanobacteria and higher plants, Phys. Chem. Chem. Phys. 6 (2004) 4838–4843. https://doi.org/10.1039/b407656g

[63] G. Christen, G. Renger, The role of hydrogen bonds for the multiphasic P_{680}^+ reduction by Y_Z in photosystem II with intact oxygen evolution capacity: analysis of kinetic H/D isotope exchange effects, Biochemistry 38 (1999) 2068–2077. https://doi.org/10.1021/bi982188t

[64] D. Béal, F. Rappaport, P. Joliot, A new high-sensitivity 10-ns time-resolution spectrophotometric technique adapted to in vivo analysis of the photosynthetic apparatus, Rev. Sci. Instrum. 70 (1999) 202–207. https://doi.org/10.1063/1.1149566

[65] M. Sugiura, T. Taniguchi, N. Tango, M. Nakamura, J. Sellés, A. Boussac, Probing the role of arginine 323 of the D1 protein in photosystem II function, Physiol. Plant. 171 (2021) 183–199. https://doi.org/10.1111/ppl.13115

[66] J-L. Zimmermann, A.W. Rutherford, Photoreductant-induced oxidation of Fe^{2+} in the electron-acceptor complex of Photosystem II, Biochim. Biophys. Acta 851 (1986) 416–423. https://doi.org/10.1016/0005-2728(86)90078-2

[67] C. Fufezan, C. Zhang, A. Krieger-Liszkay, A.W. Rutherford, Secondary quinone in Photosystem II of *Thermosynechococcus elongatus*: Semiquinone−Iron EPR signals and temperature dependence of electron transfer, Biochemistry 44 (2005) 12780–12789. https://doi.org/10.1021/bi051000k

[68] F. Rappaport, J. Lavergne, Proton release during successive oxidation steps of the photosynthetic water oxidation process - stoichiometries and pH-dependence, Biochemistry 30 (1991) 10004–10012. https://doi.org/10.1021/bi00105a027

[69] K. Brettel, E. Schlodder, H.T. Witt, Nanosecond reduction kinetics of photooxidized chlorophyll-a_{II} (P-680) in single flashes as a probe for the electron pathway, H^+-release and charge accumulation in the O_2-evolving complex, Biochim. Biophys. Acta 766 (1984) 403–415. https://doi.org/10.1016/0005-2728(84)90256-1

[70] A. Boussac, Temperature dependence of the high-spin S_2 to S_3 transition in Photosystem II: Mechanistic consequences, Biochim. Biophys. Acta 1860 (2019) 508–519. https://doi.org/10.1016/j.bbabio.2019.05.001

[71] F. Allgöwer, A.P. Gamiz-Hernandez, A.W. Rutherford, V.R.I. Kaila, Molecular principles of redox-coupled protonation dynamics in Photosystem II, J. Am. Chem. Soc. 144 (2022) 7171–7180. https://doi.org/10.1021/jacs.1c13041

[72] F. Allgöwer, M.C. Pöverlein, A.W. Rutherford, V.R.I. Kaila, Mechanism of proton release during water oxidation in Photosystem II, https://doi.org/10.1101/2024.07.03.602004

[73] T. Noguchi, Mechanism of proton transfer through the D1-E65/D2-E312 gate during photosynthetic water oxidation, J. Phys. Chem. B 128 (2024) 1866−1875. https://doi.org/10.1021/acs.jpcb.3c07787

[74] H. Dau, P. Greife, Applicability of transition state theory to the (proton-coupled) electron transfer in photosynthetic water oxidation with emphasis on the entropy of activation, Inorganics 11 (2023) 389. https://doi.org/10.3390/inorganics11100389